Performance of Optical Spatial Modulation in Indoor Multipath Channel

Performance of Optical Spatial Modulation in Indoor Multipath Channel

Hammed G. Olanrewaju, *Student Member, IEEE*, John Thompson, *Fellow, IEEE*, and Wasiu O. Popoola, *Senior Member, IEEE*

***Abstract*—In this paper, the performance of optical spatial modulation (OSM) in the indoor multipath optical wireless channel is investigated. Multipath propagation of the transmitted signal results in the temporal dispersion which causes intersymbol interference (ISI) especially in high-speed communications. OSM schemes have been investigated in line-of-sight (LOS) channels. However, given the recent trend in Gigabits per second communication, there is need to investigate the impact of the neglected higher-order reflections. Two variants of OSM are explored as case studies: optical space shift keying (OSSK) and spatial pulse position modulation (SPPM). The multipath-induced ISI is modelled to account for the spreading of the transmitted signal, and the analytical upper bound on the symbol error rate of both OSM schemes in multipath channel is derived. The derived analytical bounds are validated by closely matching simulation results. Furthermore, using the spatial distributions of the multipath-induced power penalty, the LOS channel response and the delay spread across the room, we demonstrate how the interaction between these parameters impacts error performance. Multipath-induced ISI has a significant adverse impact on the performance of OSM schemes, particularly on the detection of the activated transmitter as the incurred ISI can alter the channel gain of the received symbol.**

***Index Terms*—Wireless optical communication, spatial modulation, multipath, intersymbol interference, optical MIMO.**

I. Introduction

Optical wireless communication (OWC) has emerged as a promising candidate technology for the next generation high-speed wireless networks, complementing the existing radio frequency system with its huge bandwidth resource. Other potential benefits of OWC include energy and cost efficiency, simple front-end devices and system components, and insusceptibility to electromagnetic interference which makes it suitable for sensitive environments including hospitals, aircraft, power plant, among others [1]–[4].

Widely known modulation schemes for OWC include on-off keying (OOK), different variants of pulse position modulation (PPM) and pulse amplitude modulation (PAM) [1], [3]. In order to enhance system capacity/reliability, multiple-input multiple-output (MIMO) techniques have been used to create parallel communication channels by exploiting additional degree of freedom, such as space and emitted colour of the optical sources and field of view of detectors [5], [6]. Conventional MIMO systems utilize all the transmit units (TXs) to simultaneously send multiple data streams in order to achieve multiplexing or transmit-diversity gain. In [7], spatial modulation (SM) is introduced as a MIMO technique which activates only one of the TXs at any given time. The SM scheme encodes part of the total bits transmitted per symbol on the index of the activated TX, while the rest are conveyed by the transmitted digital signal modulation. SM has emerged as a low-complexity MIMO technique with a potential to support high data rate and energy-efficient wireless communication [8]. A detailed comparison of optical SM (OSM) technique with other MIMO techniques such as repetition coding (RC) and spatial multiplexing (SMUX) is available in [9]. In addition, different variants of OSM have been reported for OWC [10]–[15]. The differences in these variants include, but are not limited to, the number of TXs that are activated concurrently, and the type of digital signal modulation that is transmitted by the activated TXs.

Most investigations on SM-based indoor OWC have considered performance evaluation in additive white Gaussian noise channel using line-of-sight (LOS) channel response only. That is, the CIR has just a single tap [11], [12], [16]–[18]. The assumption of LOS channel is suitable for low-speed transmission systems, where the symbol duration is long enough to capture the delayed signals arriving after multiple reflections from the room surfaces. However, in recent times, high-speed Gigabits per second (Gbps) optical wireless data communications have been demonstrated [19], [20]. Due to the shorter symbol duration in high-speed communication, the multipath propagation of the transmitted signal causes temporal dispersion, otherwise known as pulse spreading. The spreading of the transmitted pulse constitutes intersymbol interference (ISI) which degrades the performance of the system [1], [21]. Moreover, several works on indoor optical channel modelling have reported the significance of multiple reflections from room surfaces [22]–[24]. Thus, the assumption of an LOS channel represents an inaccurate estimation of the system performance metric such a signal-to-noise ratio (SNR) and error rates. It is therefore imperative to examine the validity of the assumption of LOS, and to explore the neglected effect of higher order reflections.

In this paper we investigate the performance of the OSM technique in an indoor multipath OWC channel by considering two variants of OSM - optical space shift keying (OSSK) and spatial pulse position modulation (SPPM) - as case studies. The SPPM scheme [12] employs the concept of OSM to enhance the spectral efficiency of PPM while still retaining the latter's power efficiency. The spectral efficiency is improved by

H. G. Olanrewaju, J. Thompson and W. O. Popoola are with the School of Engineering, Institute for Digital Communications, LiFi R&D Centre, The University of Edinburgh, UK. E-mail: {g.olanrewaju, john.thompson and w.popoola}@ed.ac.uk. This work is supported by the Petroleum Technology Development Fund (PTDF) of the Federal government of Nigeria.

combining OSSK with PPM, and encoding additional information bits in the spatial domain of the TXs. In addition, OSSK and SPPM, like other OSM schemes, have the advantage of avoiding interchannel interference since only one TX is activated during any symbol duration.

This work provides the following novel contributions: (1) to the best of our collective knowledge, we present, for the first time, a model of the multipath-induced ISI in an OSM technique. This model accounts for the spreading of the transmitted signal due to multiple reflections from the room interior surfaces. (2) Using our ISI model, we provide the error performance analysis of SPPM in indoor multipath channel, deriving an analytical upper bound on the symbol error rate (SER) of the multipath propagation of SPPM. In addition, we show that the standard SER for the LOS propagation of SPPM, as presented in [12], can be obtained as a special case from our derived expression for SER in multipath propagation. (3) Furthermore, we extend the error performance analysis to derive the probability of symbol error for the OSSK scheme under multipath and LOS propagations. To verify the analytical model, we simulate the system performance in an indoor multipath channel with LOS and second-order reflections. The theoretical results are validated by closely matching simulation results. As indoor OWC networks are to provide full coverage and mobility, we explore the spatial distribution of system performance parameters such as channel path gain, delay spread and multipath-induced power penalty. By evaluating the performance across the entire coverage area, we demonstrate how the channel response and multipath-induced ISI impact on the error performance.

The rest of the paper is organized as follows: the descriptions of the SPPM and the OSSK schemes are given in Section II, while the system models for both schemes, as well as the configuration of the indoor OWC multipath channel are provided in Section III. In Section IV, we present a model to account for the impact of the multipath-induced ISI on the OSM schemes. The error performance analysis in multipath and LOS indoor OWC channels is given in Section V. The results of the performance evaluation are presented and discussed in Section VI, and our concluding remarks are given in Section VII.

II. Description of OSM Schemes

This section provides a brief description of the two variants of OSM technique studied in this paper, i.e., SPPM and OSSK.

A. Spatial pulse position modulation (SPPM)

Considering an optical MIMO system with N_{t} optical transmit units (TXs), i.e., light emitting diodes (LEDs), by using the SPPM signaling scheme [12], only one of the TXs is activated in a given symbol duration, while the rest of the TXs are idle. The activated source transmits an L-PPM signal pattern, where L denotes the number of time slots (chips) in a symbol duration. At the transmitter, the information bits transmitted per data symbol are grouped into two parts: the spatial bits and the signal bits. The spatial bits determine the index (position) of the TX that will be activated while the signal bits determine the position of the pulse in the PPM signal. Thus, using N_{t} TXs and L pulse positions, the total number of information bits transmitted per data symbol is $M=\log_2(N_{\mathrm{t}}L)$. The first $\log_2(N_{\mathrm{t}})$ most significant bits constitute the spatial bits, while the remaining $\log_2(L)$ bits constitute the signal bits. The SPPM scheme is further illustrated in Fig. 1 for the case of $N_{\mathrm{t}}=4$, $L=4$. For instance, to transmit the symbol '13' with binary representation '1101', the two most significant bits, '11', are used to select 'LED 4', while the last two bits, '01', indicate that the pulse will be transmitted in the second time slot of the 4-PPM pulse pattern.

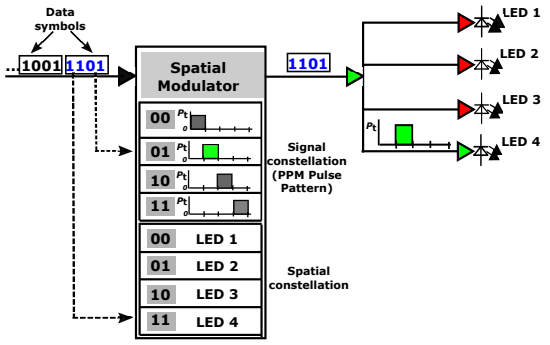

Fig. 1: An illustration of SPPM encoding using $N_{\mathrm{t}}=4$ LEDs and $L=4$.

B. Optical space shift keying (OSSK)

The OSSK scheme can be seen as a subset of the SPPM scheme. As in SPPM, only one TX is activated during a given symbol duration in OSSK. However, the activated TX does not transmit any digital signal modulation. Rather, a rectangular pulse of constant peak optical power is emitted for the entire symbol duration. Thus, in OSSK, the data symbol is encoded solely in the index of the activated TX. With N_{t} TXs, a total of $M=\log_2(N_{\mathrm{t}})$ bits are transmitted per symbol. An illustration of the OSSK signalling scheme with 4 LEDs is depicted in Fig. 2. Two information bits are transmitted per symbol, and the first two bits, '01', are sent by activating 'LED 2'.

C. Symbol detection at the receiver

As the signal emitted by the activated TX propagates through an OWC channel to the receiver (RX), due to the different spatial locations of the TXs, each TX introduces a specific "channel signature" i.e., the channel impulse response (CIR), that makes its emitted signal unique at the RX compared to the same signal emitted by any other TX. The more different the channel signatures are from each other, the more identifiable the signals from each TX become at the RX [9], [14]. At the RX, the demodulation unit exploits the unique signatures associated with each TX to estimate the transmitted symbols. The CIRs of the N_{t} TXs are assumed to be known at the RX. This can be obtained by sending pilot symbols prior to the transmission of the data symbols. Based on the estimated CIRs, the demodulator performs a maximum likelihood detection (MLD) by considering all the possible combinations of CIRs (i.e., the TX indices) and digital modulation symbols (PPM symbols), and makes a decision in favour of the combination associated with the

$$y(t) = RP_{\rm t}\sum_{\lambda=1}^{N}\sum_{k=(\lambda-1)L}^{\lambda L-1} x_k\,\delta(t-kT_{\rm c})\otimes p_{\rm T}(t)\otimes \widehat{h}_{t_\lambda}(t)\otimes p_{\rm R}(t)+z(t),\quad 0\le t\le NT \tag{2}$$

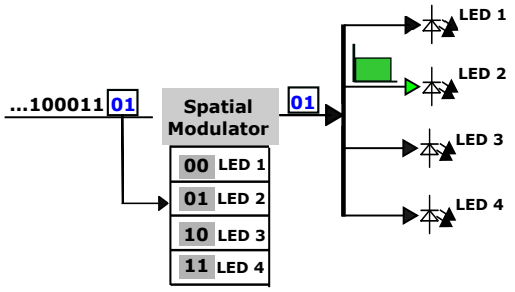

Fig. 2: An illustration of OSSK encoding using $N_{\rm t}=4$ LEDs.

lowest Euclidean distance from the actual received signal. For the OSSK scheme, the MLD is based on the CIRs (i.e., the TX indices) only.

III. System Model

In this section, using the SPPM scheme as a reference, the system model for the transmission and detection of data symbols is presented. In addition, the configuration of the indoor OWC multipath channel is provided.

A. SPPM System Model

Let $\mathbf{x}=\{\mathbf{c}_1,\ldots,\mathbf{c}_N\}$ denote a sequence of N consecutively transmitted SPPM symbols. The nth symbol, $\mathbf{c}_n$, is transmitted by activating the LED t_n to transmit a pulse in slot ℓ_n of the $L-$PPM signal, where $t_n\in[1,N_{\rm t}]$ and $\ell_n\in[0,L-1]$. Moreover, each symbol is a length-L binary chip sequence written as $\mathbf{c}_n=\{c_n^0,\ldots,c_n^q,\ldots,c_n^{L-1}\}$, and with a chip rate of $1/T_{\rm c}$, where the duration of each PPM time slot $T_{\rm c}=T/L$, and T is the SPPM symbol period. The entries of $\mathbf{c}_n$ are such that $c_n^q=1$ if $q=\ell_n$ (since the pulse is transmitted in slot ℓ_n), otherwise $c_n^q=0$. Therefore, the serialised length-LN chip sequence for the N sequentially transmitted symbols can be expressed as:

$$\begin{aligned}\mathbf{x}&=\{c_1^0,\ldots,c_1^{L-1},\ldots,c_n^0,\ldots,c_n^{L-1},\ldots,c_N^0,\ldots,c_N^{L-1}\}\\&=\{x_0,x_1,\ldots,x_k,\ldots,x_{LN-1}\}.\end{aligned}\tag{1}$$

In (1), x_k of the sequence $\mathbf{x}$ corresponds to the chip c_n^q where $k=(n-1)L+q$. The transmitted $L-$PPM optical signal is obtained by passing the chip sequence $\mathbf{x}$ through a unit-energy rectangular pulse-shaping (transmitter) filter $p_{\rm T}(t)$ of duration $T_{\rm c}$. The resulting signal is then scaled by the peak transmitted optical power $P_{\rm t}$.

Considering an OWC system with a single RX, the CIR of the subchannel from the jth TX to the RX is denoted by $\widehat{h}_j(t)$, $j=1,\ldots,N_{\mathbf{t}}$, and it includes the LOS and the multipath components. Also, $\widehat{h}_j(t)$ is assumed to be fixed, positive, and of finite duration [21]. The matched filter (MF) receiver architecture employs a unit-energy receiver filter $p_{\rm R}(t)$, which is matched to $p_{\rm T}(t)$. Hence, for the N transmitted symbols, the received electrical signal at the output of the receiver filter is given by (2). Where $\delta(.)$ is the Dirac delta function and $\otimes$ denotes the convolution operation. The parameter R is the responsivity of the photodetector (PD), while $\widehat{h}_{t_\lambda}(t)$ is the CIR of LED t_λ which is activated to send the signal of the λth symbol. The quantity $z(t)$ is the additive Gaussian noise at the receive filter output. Considering a Silicon PIN PD, $z(t)$ results from the ambient light shot noise and the thermal noise in the receiver [1]. By defining the combined impulse response of the channel, the transmitter and receiver filter as:

$$h_{t_\lambda}(t)=p_{\rm T}(t)\otimes\widehat{h}_{t_\lambda}(t)\otimes p_{\rm R}(t)\,,\tag{3}$$

the receive filter output in (2) can thus be expressed as:

$$y(t)=RP_{\rm t}\sum_{\lambda=1}^{N}\sum_{k=(\lambda-1)L}^{\lambda L-1} x_k\,h_{t_\lambda}(t-kT_{\rm c})+z(t).\tag{4}$$

The output of the MF for each of the L slot/chip of the transmitted symbols is obtained by sampling at the chip rate $1/T_{\rm c}$. The sampled version of the received signal is given by:

$$\begin{aligned}y_m&=RP_{\rm t}\sum_{\lambda=1}^{N}\sum_{k=(\lambda-1)L}^{\lambda L-1} x_k\,h_{t_\lambda}\big((m-k)T_{\rm c}\big)+z_m\\&=RP_{\rm t}\sum_{\lambda=1}^{N}\sum_{k=(\lambda-1)L}^{\lambda L-1} x_k\,h_{t_\lambda}^{m-k}+z_m,\end{aligned}\tag{5}$$

where $h_{t_\lambda}^{m-k}=h_{t_\lambda}\big((m-k)T_{\rm c}\big)$ is the $T_{\rm c}$-spaced sampled version (discrete-time (DT) representation) of the combined impulse response, and $z_m=z(mT_{\rm c})$ are the noise samples in each time slot.

For the nth received SPPM symbol, the MF samples corresponding to its L slots/chips are expressed as:

$$\begin{aligned}\mathbf{r}_n&=\mathbf{s}_n+\mathbf{w}_n\\\{r_{n,q}\}_{q=0}^{(L-1)}&=\{s_{n,q}+w_{n,q}\}_{q=0}^{(L-1)}\,,\end{aligned}\tag{6}$$

where $\{w_{n,q}\}_{q=0}^{(L-1)}$ are the L Gaussian noise samples with variance σ_w^2 and $\{s_{n,q}\}_{q=0}^{(L-1)}$ are the received signal samples in the absence of noise. By using (1), $\{r_{n,q}\}_{q=0}^{(L-1)}$ are obtained from y_m by substituting $m=(n-1)L+q$. Therefore, the magnitude of the noise-free signal samples for the nth symbol are obtained from (5) as:

$$s_{n,q}=RP_{\rm t}\sum_{\lambda=1}^{n}\sum_{k=(\lambda-1)L}^{\lambda L-1} x_k\,h_{t_\lambda}^{(n-1)L+q-k}.\tag{7}$$

The receiver makes decisions on the received symbol by determining the pulse position and the TX index combination which gives the minimum Euclidean distance metric from the received signal samples. That is, the estimate of the pulse position $\widehat{\ell}_n$ and the TX index $\widehat{t}_n$ are given by:

$$[\widehat{\ell}_n,\widehat{t}_n]=\arg\max_{q,t_n} f_n(\mathbf{r}_n|\mathbf{s}_n)=\arg\max_{q,t_n}\left[\mathcal{D}\left(\mathbf{r}_n,\mathbf{s}_n\right)\right]\tag{8}$$

The probability density function of $\mathbf{r}_n$ conditioned on $\mathbf{s}_n$ is:

$$f_w(\mathbf{r}_n|\mathbf{s}_n) = \frac{1}{(2\pi\sigma_w^2)^{L/2}} \exp\left[-\frac{\|\mathbf{r}_n - \mathbf{s}_n\|^2}{2\sigma_w^2}\right], \quad (9)$$

and the Euclidean distance metric is defined as

$$\mathcal{D}(\mathbf{r}_n, \mathbf{s}_n) = \|\mathbf{r}_n - \mathbf{s}_n\|^2. \quad (10)$$

where $\|\cdot\|$ represents the Euclidean norm. This decision process is equivalent to determining the pulse position of the transmitted PPM signal from $\widehat{\ell}_n = \arg\max_q [r_{n,q}]$, and estimating the TX index that gives the signal with the minimum Euclidean distance from the MF sample in slot $\widehat{\ell}_n$ [12].

B. Indoor Multipath Channel

In the indoor OWC channel, the transmitted optical signal experiences multipath propagation due to multiple reflections from room surfaces and other objects. The multipath CIR is obtained from simulation which is performed based on the ray-tracing algorithm in [22], [25]. The simulated channel consists of an LOS path and second-order reflections from the room surfaces. These reflections are typically diffuse in nature and are modeled as Lambertian [25]. We consider four LEDs in an empty area with the dimensions: $(5 \times 5 \times 3)$m, as shown in Fig 3. The setup configuration is designed in line with other papers on optical channel modelling [22], [23]. The configuration can however be varied to any dimension or number of sources without any loss of generality. The angle of irradiance and incidence of light rays are denoted by θ and ψ respectively, while l represents the distance covered as the optical radiation travels from one point to another, as shown in Fig 3. The simulation parameters used are provided in Table I [22]. The receiver (RX) location is varied to different coordinates across the floor of the coverage area. The values of reflectivity, ρ, are obtained from the typical measured values for different interior materials [23].

The root mean square (RMS) delay spread, $\tau_{\rm rms}$, is a measure of the pulse spreading, and thus, the ISI experienced in indoor multipath channel [1], [21]. Therefore, in this work, $\tau_{\rm rms}$ is used to quantify the amount of dispersion experienced in the multipath channel, and it is given by [1]:

$$\tau_{\rm rms} = \sqrt{\frac{\int_{-\infty}^{\infty}(t-\overline{\tau})^2\,\widehat{h}^2(t)\,\mathrm{d}t}{\int_{-\infty}^{\infty}\widehat{h}^2(t)\,\mathrm{d}t}}. \quad (11)$$

The mean delay spread, $\overline{\tau}$, is obtained from:

$$\overline{\tau} = \frac{\int_{-\infty}^{\infty} t\,\widehat{h}^2(t)\,\mathrm{d}t}{\int_{-\infty}^{\infty}\widehat{h}^2(t)\,\mathrm{d}t}. \quad (12)$$

For a multiple transmitter system, the overall delay spread of the system is defined as: $\tau_{\rm rms} = \max\left[\{\tau_{\rm rms}^j\}_{j=1}^{N_{\rm t}}\right]$, where $\tau_{\rm rms}^j$ is the RMS delay spread of the multipath link between the jth TX and the RX. Furthermore, the CIRs of all the TXs are normalised such that for the TX with the best path gain, its impulse response has unity area [22]. That is,

$$\max_{1\le j\le N_{\rm t}}\left[\int_0^{\infty}\widehat{h}_j(t)\right] = 1. \quad (13)$$

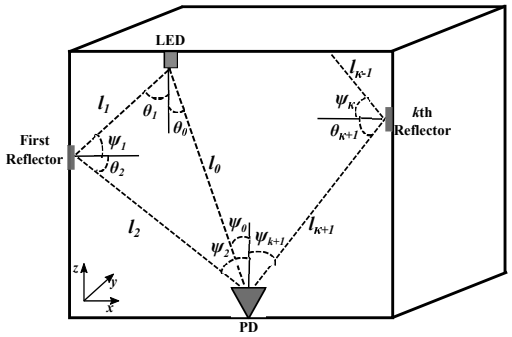

Fig. 3: Geometry of ray-tracing in an indoor OWC channel.

TABLE I:
OWC CHANNEL SIMULATION PARAMETERS

Parameter	Value
LED half angle	60°
PD field of view	85°
PD Area (cm^2)	1.0
Gain of optical filter	1.0
Concentrator index	1.5
$\rho_{\rm wall}$, $\rho_{\rm ceiling}$, $\rho_{\rm floor}$	0.83, 0.48, 0.63
Transmitters' coordinate (m)	TX1 - (1.25,1.25,3) TX2 - (1.25,3.75,3) TX3 - (3.75,1.25,3) TX4 - (3.75,3.75,3)

With this assumption, if the LOS and all the multipath component signals are captured within a single symbol duration, then, for the TX with the best channel gain, the received optical power is equal to the transmitted optical power $P_{\rm t}$.

IV. Modelling ISI Due to Multipath Propagation

Without loss of generality, let the DT combined multipath impulse response for the TXs, h_j for $j = 1, \ldots, N_{\rm t}$, have equal number of taps, $K > 1$. For the purpose of this analysis, this assumption can be implemented by zero-padding the impulse response of the TXs with a smaller number of taps. Then, the expression in (7) represents a convolution of the transmitted chip sequences from the first to the nth symbol with the DT combined impulse response of the TX that is activated to convey each symbol. This convolution operation implies that the pulse transmitted in any of the L slots/chips of a symbol will spread into other time slots. That is, due to multipath propagation, the samples of any non-zero chip will interfere with the samples of other chips within the same symbol (intrasymbol interference) and the chips in other adjoining symbols (intersymbol interference) [21]. The term ISI used in this work refers to the collective effect of these two interference cases. In the following derivation, we present a model to account for the ISI incurred in a desired symbol due to the pulse spreading from other symbols.

Let h_j^i for $i = 0, \ldots, (K-1)$, denote the amplitude of the $(i+1)$th tap of the DT combined channel response of the jth TX. By defining the tap index as a non-negative integer in the range: $0 \le i \le K-1$, then, the limits of the second summation function in (7) must satisfy the condition that:

$$0 \le (n-1)L + q - k \le K - 1. \quad (14)$$

That is, $\big((n-1)L+q-K+1\big) \leq k \leq (n-1)L+q$. Therefore, the limits of (7) are re-defined to satisfy (14), and we obtain:

$$s_{n,q} = RP_{\rm t} \sum_{\lambda=1}^{n} \sum_{k=k_{\min}}^{k_{\max}} x_k \, h_{t_\lambda}^{(n-1)L+q-k}, \tag{15}$$

where

$$\begin{aligned} k_{\min} &= \max\left[(\lambda-1)L,\, (n-1)L+q-K+1\right] \\ k_{\max} &= \min\left[(\lambda L-1),\, (n-1)L+q\right]. \end{aligned} \tag{16}$$

The functions $\max[\alpha_1, \alpha_2]$ and $\min[\alpha_1, \alpha_2]$ find the maximum and the minimum respectively between two quantities α_1 and α_2. Furthermore, for a DT impulse response with K taps, the number of slots/chips of the previously transmitted symbol(s) that are likely to interfere with the desired symbol is $(K-1)$. Hence, the number of possible ISI symbols is $N_{\rm ISI} = \left\lceil \frac{(K-1)}{L} \right\rceil$, where $\lceil \cdot \rceil$ denotes the ceiling function.

Consider a sequence of the first n consecutively transmitted symbols, $\mathbf{x} = \{\mathbf{c}_1, \ldots, \mathbf{c}_n\}$, where $n = N_{\rm ISI}+1$, the nth symbol, $\mathbf{c}_n$, is the desired symbol received in the current symbol duration while the sequence $\mathbf{x}_{\rm ISI} = \{\mathbf{c}_1, \ldots, \mathbf{c}_{n-1}\}$ represents the $(n-1)$ previously transmitted symbols that are likely to interfere with symbol $\mathbf{c}_n$. We refer to this interfering symbols as the ISI symbols. For slot q of symbol $\mathbf{c}_n$, i.e., c_n^q, let $\mathbf{d}_{n,q}$ denote a sequence of K chips consisting of the chip c_n^q and the $(K-1)$ previously transmitted chips which can constitute ISI. By using (15), the sequence $\mathbf{d}_{n,q}$ is written as:

$$\begin{aligned} \mathbf{d}_{n,q} &= \{d_{n,q}^{K-1},\, d_{n,q}^{K-2}, \ldots, d_{n,q}^{i}, \ldots, d_{n,q}^{0}\} \\ &= \left\{ \left\{ x_k \right\}_{k=k_{\min}}^{k_{\max}} \right\}_{\lambda=1}^{n}. \end{aligned} \tag{17}$$

Similarly, the sequence of the magnitude of the DT channel response for chip c_n^q and the previously transmitted $(K-1)$ chips is given by:

$$\begin{aligned} \boldsymbol{\beta}_{n,q} &= \{\beta_{n,q}^{K-1},\, \beta_{n,q}^{K-2}, \ldots, \beta_{n,q}^{i}, \ldots, \beta_{n,q}^{0}\} \\ &= \left\{ \left\{ h_{\rm t_\lambda}^{(n-1)L+q-k} \right\}_{k=k_{\min}}^{k_{\max}} \right\}_{\lambda=1}^{n}. \end{aligned} \tag{18}$$

As an illustration, considering the case of $L=4$ and $K=7$, then, $N_{\rm ISI}=2$ and $n=3$. The chips of the desired symbol $\mathbf{c}_3$ and the ISI symbols, $\mathbf{c}_1$ and $\mathbf{c}_1$, are depicted in Fig. 4. For the second slot/chip, c_3^1, of the desired symbol, using (16), (17) and (18), the sequences $\mathbf{d}_{3,1}$ and $\boldsymbol{\beta}_{3,1}$ are obtained as:

$$\mathbf{d}_{3,1} = \{d_{3,1}^{6}, d_{3,1}^{5}, \ldots, d_{3,1}^{0}\} \;=\; \{x_3,\, x_4, \ldots,\, x_9\} \tag{19}$$

$$\boldsymbol{\beta}_{3,1} = \; \{h_{t_1}^{6}, h_{t_2}^{5}, h_{t_2}^{4}, h_{t_2}^{3}, h_{t_2}^{2}, h_{t_3}^{1}, h_{t_3}^{0}\}. \tag{20}$$

Using (17) and (18), the magnitude of the noise-free signal sample received in slot q of the nth symbol, as given by (15), can be expressed in term of the sequences $\mathbf{d}_{n,q}$ and $\boldsymbol{\beta}_{n,q}$ as:

$$\begin{aligned} s_{n,q} &= RP_{\rm t} \sum_{i=0}^{K-1} d_{n,q}^{i}\, \beta_{n,q}^{i} \\ &= RP_{\rm t}\, d_{n,q}^{0}\, \beta_{n,q}^{0} \;+\; RP_{\rm t} \sum_{i=1}^{K-1} d_{n,q}^{i}\, \beta_{n,q}^{i}, \end{aligned} \tag{21}$$

for $q \in [0, L-1]$. The first term of (21), i.e., $s_{n,q}^{\rm D} = RP_{\rm t}\, d_{n,q}^{0}\, \beta_{n,q}^{0}$, represents the magnitude of the ISI-free signal sample without noise. The second term, $s_{n,q}^{\rm ISI} = RP_{\rm t} \sum_{i=1}^{K-1} d_{n,q}^{i}\, \beta_{n,q}^{i}$, accounts for the multipath-induced ISI introduced by the previously transmitted symbols. To simplify the error performance analyses that follow, we define the parameters:

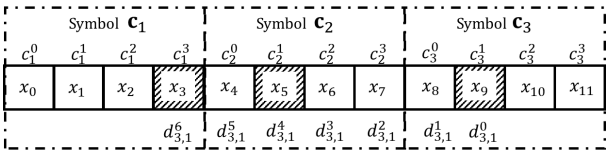

Fig. 4: A sample of chip sequence, $\mathbf{d}_{n,q}$, consisting of the chips of the desired symbol $\mathbf{c}_3$ and the chips of symbols $\mathbf{c}_1$ and $\mathbf{c}_2$ that are likely to cause ISI. $L=4$, $K=7$ and $n=3$. The shaded chips represent the pulse position of each symbol, i.e, the non-zero chips.

$$G_{n,q} = d_{n,q}^{0}\, \beta_{n,q}^{0} \tag{22}$$

$$\widehat{G}_{n,q} = \sum_{i=1}^{K-1} d_{n,q}^{i}\, \beta_{n,q}^{i}, \tag{23}$$

where $G_{n,q}$ is the DT channel response of the ISI-free signal sample, while $\widehat{G}_{n,q}$ is the combined DT channel responses of the interfering signal samples.

V. Error Performance Analysis

A transmitted symbol is correctly decoded if both the pulse position and the TX index are correctly decoded. Thus, the symbol error probability of SPPM is given by:

$$P_{\rm e,sym} \;= 1 - \left(P_{\rm c,tx} \times P_{\rm c,ppm}\right), \tag{24}$$

where $P_{\rm c,ppm}$ is the probability of correctly decoding the PPM pulse position and $P_{\rm c,tx}$ is the probability of correctly decoding the index of the activated TX given that pulse position has been correctly decoded. Considering that the desired symbol, $\mathbf{c}_n$, is transmitted by activating the jth TX to send a pulse in slot/chip μ of the L-PPM signal, i.e., $t_n \triangleq j$ and $\ell_n \triangleq \mu$, the expressions for $P_{\rm c,ppm}$ and $P_{\rm c,tx}$ are derived as follow.

A. Probability of Correct Pulse Position Detection

The pairwise error probability (PEP) that the receiver decides in favour of slot ν instead of slot μ, is the probability that the magnitude of the received signal sample in slot ν is greater than the magnitude of the sample in slot μ. That is,

$$\begin{aligned} {\rm PEP}_{\mu\to\nu}^{j} &= \mathbb{P}[s_{n,\nu} + w_{n,\nu} \;>\; s_{n,\mu} + w_{n,\mu}] \\ &= Q\left(\sqrt{\frac{\gamma_{\rm s}}{2}}\left[G_{n,\mu} + \widehat{G}_{n,\mu} - G_{n,\nu} - \widehat{G}_{n,\nu}\right]\right). \end{aligned} \tag{25}$$

The notation $\mathbb{P}[\cdot]$ represents the probability of occurrence, $Q(\cdot)$ denotes the Marcum's Q-function, and the symbol SNR, $\gamma_{\rm s} = (RP_{\rm t})^2/\sigma_w^2$. For the $N_{\rm t}$ equiprobable TXs which could be activated to send the desired symbol, using the union bound techniques [26] with equation (25), the probability of error in detecting the pulse position is obtained as:

$$P_{\rm e,ppm} \leq \frac{1}{LN_{\rm t}} \sum_{j=1}^{N_{\rm t}} \sum_{\mu=0}^{L-1} \sum_{\substack{\nu=0 \\ \nu\neq\mu}}^{L-1} {\rm PEP}_{\mu\to\nu}^{j}. \tag{26}$$

$$\mathrm{PEP}_{\mu}^{j\to\kappa}=\mathbb{P}\Big[\big(s_{n,\mu}^{\mathrm{ISI},j}+w_{n,\mu}\big)^2>\big(s_{n,\mu}^{\mathrm{D},j}+s_{n,\mu}^{\mathrm{ISI},j}+w_{n,\mu}-s_{n,\mu}^{\mathrm{D},\kappa}\big)^2\Big]=Q\left(\sqrt{\frac{\gamma_{\mathrm{s}}}{4}}\left[\frac{\big(G_{n,\mu}^{j}-G_{n,\mu}^{\kappa}\big)\times\big(G_{n,\mu}^{j}-G_{n,\mu}^{\kappa}+2\widehat{G}_{v}^{j}\big)}{\Big|G_{n,\mu}^{\kappa}-G_{n,\mu}^{j}\Big|}\right]\right) \quad (29)$$

The average probability of error in pulse position detection is obtained by averaging $P_{\mathrm{e,ppm}}$ over: (i) all the $(N_{\mathrm{t}})^{(n-1)}$ possible combinations of LEDs, $\{\mathbf{t}_{\mathrm{ISI}}\}=\{t_1,\ldots,t_{n-1}\}$, that are activated to send the ISI symbols, and (ii) all the $L^{(n-1)}$ combinations of chip sequences, $\{\mathbf{x}_{\mathrm{ISI}}\}=\{x_0,\ldots,x_{L(n-1)-1}\}$ for the ISI symbols. Therefore, the probability of correct pulse position detection is obtained as:

$$P_{\mathrm{c,ppm}}=1-\frac{1}{(LN_{\mathrm{t}})^{(n-1)}}\sum_{\{\mathbf{t}_{\mathrm{ISI}}\}}\sum_{\{\mathbf{x}_{\mathrm{ISI}}\}}P_{\mathrm{e,ppm}}. \quad (27)$$

B. Probability of Correct Transmitter Detection

For the desired symbol $\mathbf{c}_n$, for a correctly detected pulse position, i.e., $\widehat{\mu}=\mu$, the PEP that the receiver decides in favour of LED κ instead of j, is obtained as:

$$\begin{aligned}\mathrm{PEP}_{\mu}^{j\to\kappa}&=\mathbb{P}\big[D(r_{n,\mu},s_{n,\mu}^{\mathrm{D},j})>D(r_{n,\mu},s_{n,\mu}^{\mathrm{D},\kappa})\big]\\&=\mathbb{P}\Big[\big(r_{n,\mu}-s_{n,\mu}^{\mathrm{D},j}\big)^2>\big(r_{n,\mu}-s_{n,\mu}^{\mathrm{D},\kappa}\big)^2\Big] \quad (28)\end{aligned}$$

where $s_{n,\mu}^{\mathrm{D},j}$ and $s_{n,\mu}^{\mathrm{D},\kappa}$, represent the expected noise- and ISI-free magnitude of the MF sample for slot μ if the desired symbol is sent by TXs j and κ respectively. By applying (6) and (21) in (28), the PEP of the TX detection is given by (29). Where $G_{n,\mu}^{\kappa}\neq G_{n,\mu}^{j}$, and the parameters $G_{n,\mu}^{j}$ and $\widehat{G}_{n,\mu}^{j}$ are the values of $G_{n,\mu}$ and $\widehat{G}_{n,\mu}$ obtained from (22) and (23) respectively when the desired symbol is sent by the jth LED.

Now, considering the N_{t} equiprobable TXs, the upper bound on the probability of error in detecting the TX index is:

$$P_{\mathrm{e,tx}}\leq\frac{1}{N_{\mathrm{t}}}\sum_{j=1}^{N_{\mathrm{t}}}\sum_{\substack{\kappa=1\\\kappa\neq j}}^{N_{\mathrm{t}}}\mathrm{PEP}_{\mu}^{j\to\kappa}. \quad (30)$$

Similar to the case of the pulse position detection in Section V-A, the probability of TX detection error obtained in (30) is averaged over all the L possible positions of slot μ, over all the possible combinations of the TXs that are activated to send the ISI symbols, and over all the possible combinations of chip sequences of the ISI symbols. Thus, the probability of correctly detecting the TX index, conditioned on a correctly detected pulse position, is obtained as:

$$P_{\mathrm{c,tx}}=1-\frac{1}{L^n(N_{\mathrm{t}})^{(n-1)}}\sum_{\{\mathbf{t}_{\mathrm{ISI}}\}}\sum_{\{\mathbf{x}_{\mathrm{ISI}}\}}\sum_{\mu=0}^{L-1}P_{\mathrm{e,tx}}. \quad (31)$$

The expressions in (27) and (31) are used to evaluate (24) in order to obtain the SER of SPPM in multipath channel.

C. Special Case of LOS Propagation of SPPM

For signal transmission involving only LOS propagation, the DT combined impulse response of the TXs will have only one tap, i.e., $K=1$. As such, $h_j=h_j^0\ \ \forall j$, where h_j^0 is the LOS DT channel response of the jth TX. Thus, $N_{\mathrm{ISI}}=0$, $n=1$ and the desired symbol: $\mathbf{c}_n\triangleq\mathbf{c}_1$. Also, (16) yields $k=k_{\min}=k_{\max}=q$, and (17) and (18) reduce to:

$$\mathbf{d}_{n,q}=\ d_{1,q}^0=x_q=c_1^q,\quad \text{for } q\in[0,L-1] \quad (32)$$

$$\boldsymbol{\beta}_{n,q}=\ \beta_{1,q}^0=h_{\mathrm{t}_1}^0. \quad (33)$$

Therefore, (22) and (23) yield:

$$G_{1,q}=h_{\mathrm{t}_1}^0c_1^q;\quad \widehat{G}_{1,q}=0. \quad (34)$$

If the symbol $\mathbf{c}_1$ is conveyed by activating the TX j to transmit a pulse in slot μ, then the transmitted chip sequence is such that $c_1^q=1$ if $q=\mu$, otherwise, $c_1^q=0$. Thus, $G_{1,\mu}=h_j^0$ and $G_{1,q}=0,\ \forall q,\ q\neq\mu$. Hence, for LOS propagation, by applying (34) in (25), the PEP that the receiver decides in favour of slot ν instead of μ, is:

$$\overline{\mathrm{PEP}}_{\mu\to\nu}^{j}=Q\Big(G_{1,\mu}\sqrt{\gamma_{\mathrm{s}}}\Big)=Q\bigg(h_j^0\sqrt{\frac{\gamma_{\mathrm{s}}}{2}}\bigg). \quad (35)$$

For L equally likely slots/chips, since the chip sequence of the ISI symbols is empty, then the probability of correct pulse position detection in an LOS scenario is:

$$P_{\mathrm{c,ppm}}^{\mathrm{LOS}}=1-\frac{(L-1)}{N_{\mathrm{t}}}\sum_{j=1}^{N_{\mathrm{t}}}Q\bigg(h_j^0\sqrt{\frac{\gamma_{\mathrm{s}}}{2}}\bigg). \quad (36)$$

Similarly, by using (34) in (29), the PEP that the receiver decides in favour of TX κ instead of TX j, is given by:

$$\overline{\mathrm{PEP}}_{\mu}^{j\to\kappa}=Q\bigg(\sqrt{\frac{\gamma_{\mathrm{s}}}{4}}\Big|G_{1,\mu}^{\kappa}-G_{1,\mu}^{j}\Big|\bigg)=Q\bigg(\big|h_{\kappa}^0-h_j^0\big|\sqrt{\frac{\gamma_{\mathrm{s}}}{4}}\bigg). \quad (37)$$

Hence, the probability of correctly decoding the TX index, conditioned on a correctly decoded pulse position, is:

$$P_{\mathrm{c,tx}}^{\mathrm{LOS}}=1-\frac{1}{N_{\mathrm{t}}}\sum_{j=1}^{N_{\mathrm{t}}}\sum_{\substack{\kappa=1\\\kappa\neq j}}^{N_{\mathrm{t}}}Q\bigg(\big|h_{\kappa}^0-h_j^0\big|\sqrt{\frac{\gamma_{\mathrm{s}}}{4}}\bigg). \quad (38)$$

By combining (36) and (38), the SER for an SPPM scheme involving only LOS propagation is given by (39). The expression in (39) matches the standard expression for the SER of SPPM in LOS-only propagation as in [12, Eq. (23)].

D. Special Case of OSSK in Multipath Channel

In this section, the error performance analysis for SPPM presented above is applied to derive the theoretical SER of OSSK in indoor OWC multipath channel. In OSSK, since $L=1$, then each symbol has just a single chip/slot, i.e., $q=0$ and thus, $\mathbf{c}_u\triangleq c_u^0,\ \forall u$. Considering an n consecutively

$$P_{\mathrm{e,sym}}^{\mathrm{LOS}} \leq 1 - \left[1 - \frac{1}{N_{\mathrm{t}}}\sum_{j=1}^{N_{\mathrm{t}}}\sum_{\substack{\kappa=1\\ \kappa\neq j}}^{N_{\mathrm{t}}} Q\left(\left|h_{\kappa}^{0} - h_{j}^{0}\right|\sqrt{\frac{\gamma_{\mathrm{s}}}{4}}\right)\right] \times \left[\frac{(L-1)}{N_{\mathrm{t}}}\sum_{j=1}^{N_{\mathrm{t}}}\left[\frac{1}{L-1} - Q\left(h_{j}^{0}\sqrt{\frac{\gamma_{\mathrm{s}}}{2}}\right)\right]\right]. \quad (39)$$

transmitted OSSK symbol, $\mathbf{x}=\{\mathbf{c}_1,\ldots,\mathbf{c}_n\}$, the serialised sequence of the transmitted chips/symbols is written as:

$$\begin{aligned}\mathbf{x} &= \{x_0, x_1, \ldots, x_k, \ldots, x_{n-1}\}\\ &= \{c_1^0, c_2^0, \ldots, c_u^0, \ldots, c_n^0\},\end{aligned} \quad (40)$$

where $k \triangleq u-1$, i.e., $x_k = c_{k+1}^0$. Using the ISI model developed for SPPM in Section IV, for the DT combined impulse responses with $(K \geq 1)$ taps, the number of ISI symbols is equal to the number of interfering chips, and it is given by $N_{\mathrm{ISI}} = K-1$. Considering that the nth OSSK symbol, c_n^0, is the desired symbol received in the current symbol duration, where $n = N_{\mathrm{ISI}} + 1 = K$, then $\mathbf{x}_{\mathrm{ISI}} = \{c_1^0, c_2^0, \ldots, c_{n-1}^0\}$ represents the $(K-1)$ previously transmitted ISI symbols. Therefore, the sequence $\mathbf{d}_{n,q}$ in (17), reduces to:

$$\mathbf{d}_n = \{d_n^{K-1}, d_n^{K-2}, \ldots, d_n^0\} = \left\{\left\{x_k\right\}_{k=k_{\min}}^{k_{\max}}\right\}_{\lambda=1}^{n}. \quad (41)$$

Using $L=1$ and $q=0$ in (16), we obtain:

$$k_{\min} = \max\left[\lambda - 1, n-K\right] \quad (42a)$$

$$k_{\max} = \min\left[\lambda - 1, n-1\right]. \quad (42b)$$

Now, since in (41), $1 \leq \lambda \leq n$, then $\lambda - 1 \leq n-1$ and therefore, (42b) yields $k_{\max} = \lambda - 1$. Moreover, given that each symbol has just one chip, then $k = k_{\min} = k_{\max} = \lambda - 1$. This implies that in (42a), $\max\left[\lambda-1, n-K\right] = \lambda - 1$. Hence, $\lambda - 1 \geq n-K$ and $\lambda \geq n-K+1$. Therefore, (41) becomes:

$$\mathbf{d}_n = \left\{x_{\lambda-1}\right\}_{\lambda=n-K+1}^{n} \quad (43)$$

Similarly, the sequence of the DT combined channel response corresponding to the desired and the ISI symbols is given by:

$$\boldsymbol{\beta}_n = \{\beta_{n,q}^{K-1}, \beta_{n,q}^{K-2}, \ldots, \beta_{n,q}^{0}\} = \left\{h_{\mathrm{t}_\lambda}^{n-\lambda}\right\}_{\lambda=n-K+1}^{n}. \quad (44)$$

Let the desired symbol, $\mathbf{c}_n$ be sent by activating TX j, i.e., $t_n \triangleq j$. By using (43) and (44), the noise- and ISI-free magnitude of the MF sample for the desired symbol, is:

$$s_n^{\mathrm{D}} = RP_{\mathrm{t}}\, d_n^0\, \beta_n^0 \;=\; G_n R P_{\mathrm{t}}. \quad (45)$$

and the ISI contributed by the previously transmitted symbols is expressed as:

$$s_n^{\mathrm{ISI}} = RP_{\mathrm{t}} \sum_{i=1}^{K-1} d_n^i\, \beta_n^i \;=\; \widehat{G}_n R P_{\mathrm{t}}. \quad (46)$$

By combining (45) and (46), the magnitude of the received sample for the desired symbol is:

$$r_n = s_n^{\mathrm{D}} + s_n^{\mathrm{ISI}} + w_n = RP_{\mathrm{t}}\left(G_n + \widehat{G}_n\right) + w_n, \quad (47)$$

and the PEP that the receiver decides in favour of TX κ instead of j, is given by:

$$\mathcal{P}^{j\to\kappa} = \mathbb{P}\left[\mathcal{D}(r_n, s_n^{\mathrm{D},j}) > \mathcal{D}(r_n, s_n^{\mathrm{D},\kappa})\right]. \quad (48)$$

Therefore,

$$\mathcal{P}^{j\to\kappa} = Q\left(\sqrt{\frac{\gamma_{\mathrm{s}}}{4}}\left[\frac{\left(G_n^j - G_n^\kappa\right)\times\left(G_n^j - G_n^\kappa + 2\widehat{G}_n^j\right)}{\left|G_n^\kappa - G_n^j\right|}\right]\right) \quad (49)$$

where $G_n^\kappa \neq G_n^j$. Since signal modulation is not transmitted by the activated TX in OSSK, then, a transmitted symbol is correctly decoded if the TX index detected correctly. Thus, the symbol error probability of an OSSK scheme is equal to the probability of error in detecting the TX. Now, considering the N_{t} equally likely TXs, by averaging over all the $(N_{\mathrm{t}})^{(K-1)}$ possible combinations of the TXs that can be activated to send the ISI symbols, $\{\mathbf{t}_{\mathrm{ISI}}\} = \{t_1, \ldots, t_{K-1}\}$, the average symbol error probability of an OSSK scheme in multipath channel is:

$$P_{\mathrm{e,sym}}^{\mathrm{OSSK}} \leq \frac{1}{(N_{\mathrm{t}})^K}\sum_{\{\mathbf{t}_{\mathrm{ISI}}\}}\sum_{j=1}^{N_{\mathrm{t}}}\sum_{\substack{\kappa=1\\ \kappa\neq j}}^{N_{\mathrm{t}}}\mathcal{P}^{j\to\kappa}. \quad (50)$$

For the LOS propagation of the OSSK scheme, by setting $K=1$, we obtain $\widehat{G}_n^j = 0$, and the SER is given by:

$$P_{\mathrm{e,sym}}^{\mathrm{OSSK,LOS}} \leq \frac{1}{N_{\mathrm{t}}}\sum_{j=1}^{N_{\mathrm{t}}}\sum_{\substack{\kappa=1\\ \kappa\neq j}}^{N_{\mathrm{t}}} Q\left(\left|h_{\kappa}^{0} - h_{j}^{0}\right|\sqrt{\frac{\gamma_{\mathrm{s}}}{4}}\right). \quad (51)$$

VI. Results and Discussions

The results of the performance evaluation of the SPPM and the OSSK schemes in indoor multipath channel are presented in this section. The analytical results are obtained by using the theoretical expressions derived in Sections V, and these are validated by simulation results obtained using MATLAB.

To illustrate the performance of SPPM and without any loss of generality, we consider: $N_{\mathrm{t}} = [2, 4]$ and $L = [2, 8]$, RX coordinate: $(x, y, z) = (1.8, 2, 0)$m, and the TX coordinates as provided in Table I. For a fair comparison, the system is designed to achieve equal bit rate for all values of L. For the case of $N_{\mathrm{t}} = 2$, using transmitters TX1 and TX4, the plots of the SER against the SNR per bit, $\gamma_{\mathrm{b}} = \gamma_{\mathrm{c}}/M$, are depicted in Fig. 5. It can be seen that the derived upper bound on the SER of SPPM in multipath channel is closely matched by the simulation results, and thus validates our theoretical derivation. The SER values greater than 1, as well as the slight deviations observed between the theoretical and simulation results at SER $> 10^{-2}$, is due to the union bound technique used in the analysis. The closed form expression derived in Section V can therefore be used to study the performance of SPPM in more realistic indoor channel taking into account the multiple reflections of the transmitted signal. Moreover, the analytical framework can be easily extended to explore the performance of other OSM schemes in multipath channels.

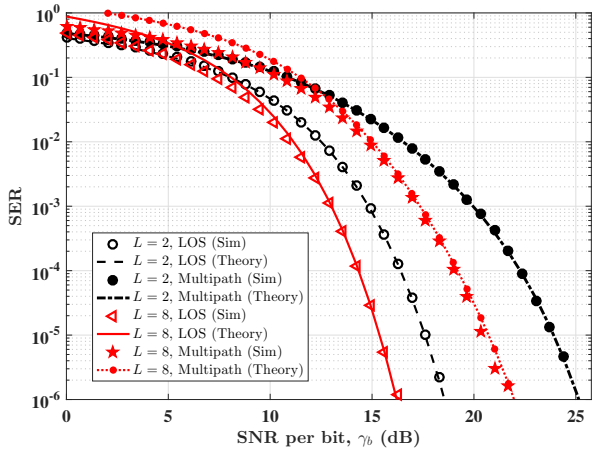

Fig. 5: Error performance of SPPM in LOS and multipath channel. $N_\mathrm{t} = 2$, $L = [2, 8]$. $\tau_\mathrm{rms} = 0.14T_\mathrm{c}$ and $0.29T_\mathrm{c}$ for $L{=}2$ and $L{=}8$ respectively. LOS channel gains: $[h_1^0, h_4^0] = [1, 0.3866]$.

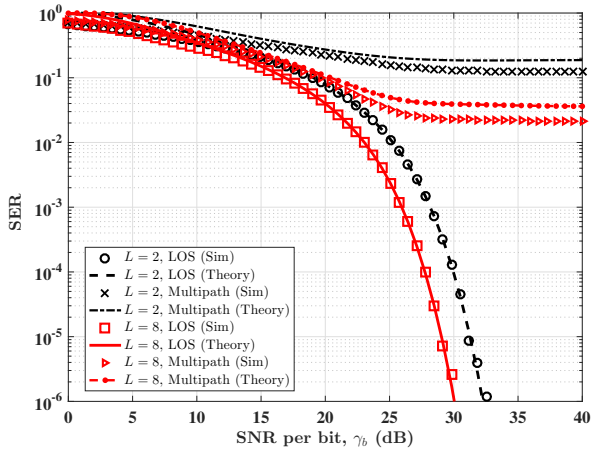

Fig. 6: Error performance of SPPM in LOS and multipath channel. $N_\mathrm{t} = 4$, $L = [2, 8]$. $\tau_\mathrm{rms} = 0.12T_\mathrm{c}$ and $0.29T_\mathrm{c}$ for $L = 2$ and $L = 8$ respectively. LOS channel gains: $\{h_j^0\}_{j=1}^{N_\mathrm{t}} = [1, 0.6365, 0.5448, 0.3866]$.

At the specified TXs and RX locations, $\tau_\mathrm{rms} = 2.32$ ns, which is equivalent to $0.14T_\mathrm{c}$ and $0.29T_\mathrm{c}$ for $L{=}2$ and $L{=}8$ respectively. Note that delay spread, τ_rms, as a function of T_c, amounts to the significance of the ISI, and not the actual value of the coherence time of the channel. For example, $\tau_\mathrm{rms}{=}0$ means T_c is greater than channel coherence time, and thus, no ISI at all. However, $\tau_\mathrm{rms}{>}0$ indicates the presence of ISI and T_c is less than the channel coherence time. Due to the dispersion experienced in multipath channel, a higher value of SNR is required to achieve a given SER in multipath compared to LOS propagation. The increase in SNR is required to overcome the multipath-induced ISI. We define SNR penalty, $\Delta\gamma_\mathrm{b}{=}\gamma_{\mathrm{b,MP}}{-}\gamma_{\mathrm{b,LOS}}$, where $\gamma_{\mathrm{b,LOS}}$ and $\gamma_{\mathrm{b,MP}}$ represent the SNR required to achieve a given value of SER under LOS and propagation respectively. For a representative SER of 10^{-5}, due to ISI, multipath propagation incurs an SNR penalty of about 6.5 dB and 5.5 dB for $L{=}2$ and $L{=}8$ respectively.

Similarly, the error performance plots for case of $N_\mathrm{t}{=}4$ are shown in Fig. 6. It is observed that the degradation in performance is more pronounced for $N_\mathrm{t} = 4$ compared to $N_\mathrm{t} = 2$. This is not unexpected because as the total number of TXs increases, the denser the spatial constellations become and the wider the variation in the magnitude and the extent of the ISI caused by the previously transmitted symbols. In particular, the denser constellations implies that SNR requirement will increase substantially. Moreover, as N_t increases, the requirement for distinct channel response for all the TXs becomes more stringent. Thus, due to ISI, there is an increasing likelihood that a small alteration in the actual channel response of the transmitted symbol will result in wrong TX detection. This is why for the case of $N_\mathrm{t} = 4$ shown in Fig. 6, even at high SNR where the limiting effect of the noise has been greatly reduced, the alteration of channel response due to ISI can cause the receiver to repeatedly decode some sets of symbols erroneously, and this keeps the SER at an irreducible level.

Using the derived SER for OSSK scheme (see Section V-D), the SER plots for the case $N_\mathrm{t}{=}2$ are shown in Fig. 7. The RMS delay spread is normalised by the symbol duration T,

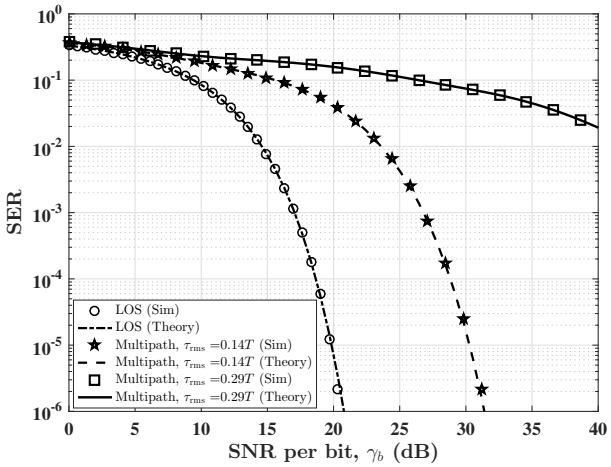

Fig. 7: Error performance of OSSK in LOS and multipath channel. $N_\mathrm{t} = 2$, $\tau_\mathrm{rms} = 0.14T$ and $0.29T$. LOS channel gains: $[h_1^0, h_4^0] = [1, 0.3866]$, SNR per bit, $\gamma_\mathrm{b}{=}\gamma_\mathrm{s}/M$.

and the SER plots for LOS propagation and two different symbol rates are shown. The derived analytical upper bound is closely matched by the simulation results. As expected, as the data rate increases, the error performance of the system degrades. This is due to the fact that as the data rate increases, the symbol duration reduces, and thus the ISI caused by the spreading of the transmitted pulse becomes more significant.

In Fig. 8, the SNR, $\gamma_{\mathrm{b,MP}}$, required to achieve SER of 10^{-5} in multipath channel is plotted against the normalised RMS delay spread, $\tau_\mathrm{rms}/T_\mathrm{c}$. For this case, $N_\mathrm{t}{=}2$, $L{=}[2, 4, 8]$ and RX coordinate: $(x, y, z){=}(0.6, 1.8, 0)$ m. The OSSK scheme and all the SPPM configurations are implemented with the same bitrate and average transmitted optical power. As L increases from 2 to 8, SPPM benefits from the increasing energy efficiency in terms of SNR. However, the SNR penalty incurred in multipath channel also increases due to the increasing bandwidth requirement. Moreover, As L increases, the duration of each PPM time slot decreases, and as a result, the probability of intrasymbol interference due to pulse spreading increases. Thus, the energy saving achieved by using a given value of L can be lost to multipath penalty if the delay spread exceeds a certain threshold. For instance, in Fig. 8,

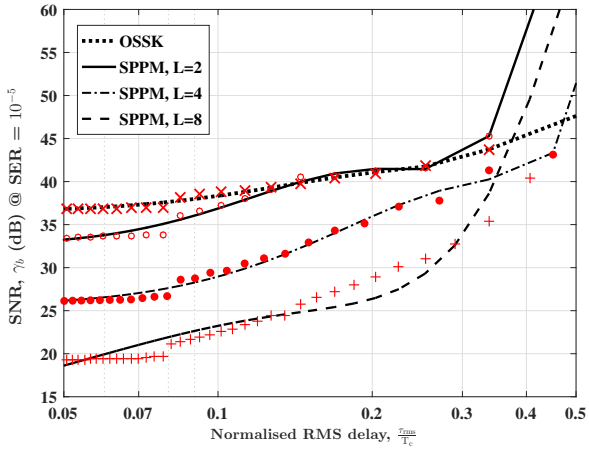

Fig. 8: SNR, $\gamma_{\mathrm{b,MP}}$, required to achieve SER of 10^{-5} in multipath channel versus RMS delay spread divided by chip duration T_{c}. The lines represent fifth-order polynomial fits to the data (Markers) for each scheme.

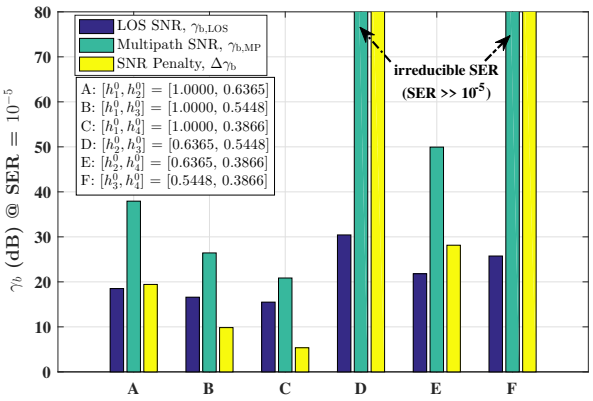

Fig. 9: SNR requirement in LOS and multipath channel for different TX pairs. $N_{\mathrm{t}} = 2$, $L = 8$.

for $\tau_{\mathrm{rms}} > 0.35T_{\mathrm{c}}$ and $\tau_{\mathrm{rms}} > 0.38T_{\mathrm{c}}$, the SNR required for $L = 8$ exceeds those $L = 4$ and $L = 2$ respectively.

In SM, correct symbol detection requires an accurate detection of the TX index, hence, the system performance is highly dependent on the identifiability of the multiple channels. In Fig. 9, we illustrate how this impacts on the performance in multipath channels. For an SPPM configuration with $L=8$, using a pair of TXs at different positions, Fig. 9 depicts the SNR required to attain an SER of 10^{-5} in LOS and multipath channels. Also included in Fig. 9, is the SNR penalty suffered in the multipath channel compared to the LOS channel. The normalised LOS path gain of the four TXs are: $\{h_j^0\}_{j=1}^{N_{\mathrm{t}}} = [1, 0.6365, 0.5448, 0.3866]$. It is observed that for both LOS and multipath channels, as the difference between the channel responses of the two TXs narrows, the required SNR increases. However, the increase in SNR is significantly higher for multipath than for LOS channels. For instance, the difference between the required SNR for the gain sets A ($[h_1^0, h_2^0] = [1, 0.6365]$) and C ($[h_1^0, h_4^0] = [1, 0.3866]$) is about 3 dB for the LOS channel compared to about 14 dB for multipath channel. The higher SNR requirement in multipath can be attributed to the fact the ISI incurred in multipath channel also alters the actual channel response for the received signal, thereby making the received symbol appear as though it had been sent by another TX. Thus, even if the pulse position can be estimated from the received amplitude when compared to the unfilled slots, the multipath-induced ISI could still cause erroneous TX detection. For less distinct channel responses, the incurred ISI can readily overcome the path gain difference to cause transmitter detection errors. As an example, for case D with a gain difference of $\left|h_2^0 - h_3^0\right| = 0.0917$, TX2 can be wrongly detected as TX3 if the combined gains of all the interfering samples exceed about half of this gain difference. Hence, even at high SNR, the SER reaches an irreducible level because the receiver continues to decode the TX index of some sets of symbols erroneously. This corroborates the widely reported dependence of OSM schemes on path gain dissimilarity [9], [27], and highlights the significant adverse impact of multipath ISI on the system performance.

As indoor OWC networks are to provide coverage and mobility, we explore the spatial distribution of system performance parameters such as channel response, delay spread and multipath-induced power penalty across the entire area of the room. The SPPM system has $N_{\mathrm{t}} = 2$ (TX1 and TX4) and $L = 8$, and the RX is positioned at different locations across the room. The spatial distributions of $\Delta\gamma_{\mathrm{b}}$ and τ_{rms} are shown in Fig. 10a and 10b respectively. Also, Fig. 10c shows the absolute difference, Δh, between the normalised LOS channel response of both TXs, i.e., $\Delta h = \left|h_1^0 - h_4^0\right|$. Given the symmetry of the configuration, similar plots can be obtained for TX2 and TX3. As observed in Fig. 10, multipath propagation make impacts differently at different locations. The delay spread is highest if the RX is positioned in the vicinity of any of the two TXs. This is because if the RX is located close to TX1 for example, then even though TX1 will have a low value of τ_{rms}, the value of τ_{rms} will be high for TX4 because it is farther from the RX. Thus, as shown in Fig. 10a, the SNR penalty in the vicinity of the both TXs are very high due to the increase in multipath-induced ISI. Along the centre of the room where the RX is equidistant from both TXs, τ_{rms} has a relative lower value (about 1.7 ns, see Fig. 10b). However, because the LOS channel responses are identical in this area of the room, $0.1 \leq \Delta h \leq 0$ (see Fig. 10c), the corresponding value of $\Delta\gamma_{\mathrm{b}}$ shown in Fig. 10a is very high. In fact, the SER lies in the range: $0.02 < \mathrm{SER} \leq 0.5$. This observation is not unexpected since SM techniques, like most MIMO techniques, are highly dependent on the identifiability of the multiple channels. As an SM technique, SPPM performs better when both Δh and the individual channel response values are optimized [12], [27].

To further demonstrate the how the interaction between channel response and multipath-induced ISI impacts on the performance, we extract the 2-dimensional plots in Fig. 11 from the contour plots of Fig. 10. The receiver is positioned at different points along the y-axis, while the x coordinate is fixed at 2.0 m. Figure 11a depicts Δh and τ_{rms} on the left and right y-axis respectively. Figure 11b depicts the plot of $\gamma_{\mathrm{b,LOS}}$ and $\gamma_{\mathrm{b,MP}}$ required to achieve a representative SER of 10^{-5}. In Fig. 11, it is observed that in the range: $0 \leq Y \leq 2$ m, as Δh reduces from 0.8 to 0.56, $\gamma_{\mathrm{b,LOS}}$ reduces gradually from about 23 dB to its lowest value of 15 dB. In this same range, however, the graph of $\gamma_{\mathrm{b,MP}}$, shows

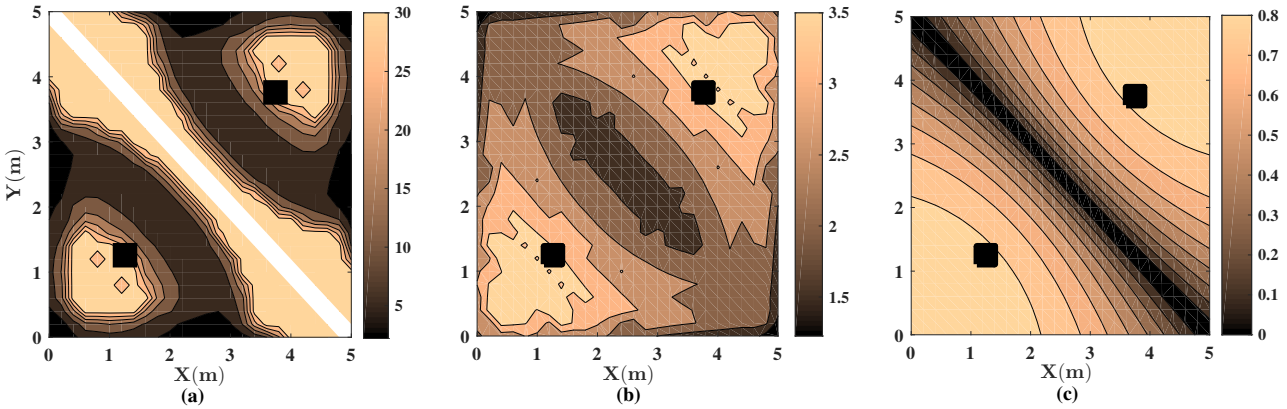

Fig. 10: Distribution of (a) SNR penalty, $\Delta\gamma_{\rm b}$ (dB), (b) RMS delay spread $\tau_{\rm rms}$ (nsec), and (c) Δh, across the room. $N_{\rm t}=2$, $L=8$. The square markers indicate the position of transmitters TX1 and TX4. The white regions in (a) indicate the RX locations at which SER $\gg 10^{-5}$

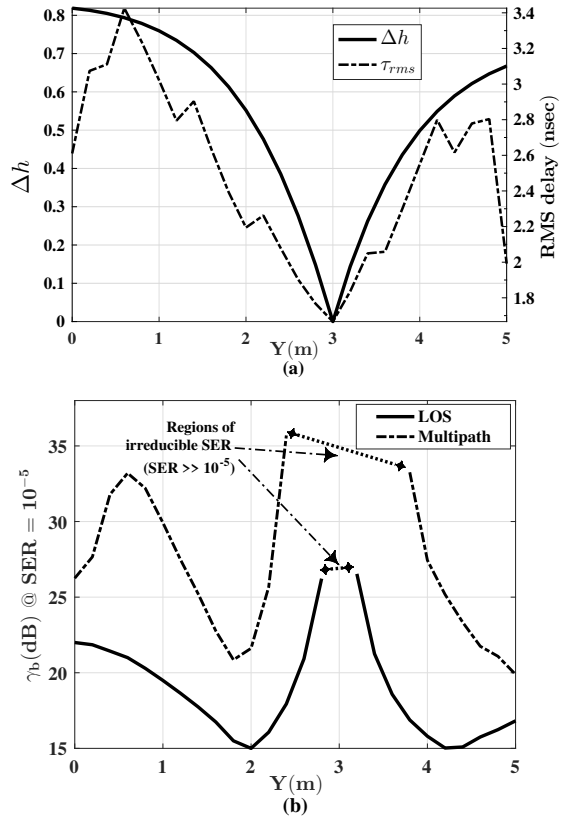

Fig. 11: (a) Plot of Δh and $\tau_{\rm rms}$ (b) Plots of $\gamma_{\rm b,LOS}$ and $\gamma_{\rm b,MP}$, for different receiver locations along the y-axis at $X = 2.0$ m. $N_{\rm t} = 2$ and $L = 8$.

a trend that follows $\tau_{\rm rms}$ rather than Δh. This is indicated by the similarity between the slopes of the graphs for $\gamma_{\rm b,MP}$ and $\tau_{\rm rms}$. On the contrary, in the range: $2 \leq Y \leq 3$, even though $\tau_{\rm rms}$ continued to decrease from about 2.2 to 1.6 ns, $\gamma_{\rm b}^{\rm mp}$ shows an opposite trend by increasing from about 21 dB into the region of irreducible SER ($0.02 < {\rm SER} \leq 0.5$). The observed trend for $\gamma_{\rm b,MP}$ is similar to that of $\gamma_{\rm b,LOS}$, and this indicates the dominance of the Δh component over the multipath ISI. As Δh decreases, the dissimilarity between the channel responses reduces, thereby making the transmitted symbol indistinguishable at the receiver. The performance of SPPM is largely dictated by the channel response values and the difference between these values. However, the ISI caused by multipath dispersion can adversely impact the identifiability of the subchannels by altering the channel response values.

VII. Conclusion

In this work, using SPPM and OSSK as case studies, the performance of optical SM in an indoor multipath channel has been studied. A model of the multipath-induced ISI in an OSM technique is presented. The model accounts for the spreading of the transmitted signal due to multiple reflections from room surfaces. The ISI model is then used to derive the analytical upper bounds on the SER of SPPM and OSSK under multipath propagation. Using a simulated indoor multipath channel with LOS and second-order reflections from the room surfaces, our theoretical derivations are validated by closely matching simulation results. The analysis presented in this work can be adopted to study the performance of OSM schemes in more realistic indoor channel taking into consideration the impact of the multipath propagation of the transmitted signal. the Multipath-induced ISI has significant impact on the performance of OSM schemes particularly on the detection of the activated transmitters. The incurred ISI can alter the actual channel response of the received symbol, thus making it appear as though it had been sent by a different transmitter. In addition, to demonstrate how multipath propagation affects coverage and mobility, we presented the spatial distribution of channel response, RMS delay spread and multipath-induced SNR penalty across the room. Results show how multipath propagation impacts system performance at different locations. The performance of SPPM is largely dictated by the channel response values and the difference between these values. However, the ISI caused by multipath dispersion can adversely impact the identifiability of the multiple channels by altering the channel response values.

References

[1] Z. Ghassemlooy, W. Popoola, and S. Rajbhandari, *Optical Wireless Communications: System and Channel Modelling with Matlab®*. CRC Press, 2012.

[2] A. Sevincer, A. Bhattarai, M. Bilgi, M. Yuksel, and N. Pala, "LIGHTNETs: Smart LIGHTing and Mobile Optical Wireless NETworks—A Survey," *IEEE Communications Surveys & Tutorials*, vol. 15, no. 4, pp. 1620–1641, 2013.

[3] D. Karunatilaka, F. Zafar, V. Kalavally, and R. Parthiban, "LED Based Indoor Visible Light Communications: State of the Art," *IEEE Communications Surveys & Tutorials*, vol. 17, no. 3, pp. 1649–1676, 2015.
[4] W. O. Popoola, "Impact of VLC on Light Emission Quality of White LEDs," *Journal of Lightwave Technology*, vol. 34, no. 10, pp. 2526–2532, May 2016.
[5] L. Zeng, D. C. O'Brien, H. Le Minh, G. E. Faulkner, K. Lee, D. Jung, Y. Oh, and E. T. Won, "High Data Rate Multiple Input Multiple Output (MIMO) Optical Wireless Communications Using White LED Lighting," *IEEE Journal on Selected Areas in Communications*, vol. 27, no. 9, 2009.
[6] K. D. Dambul, D. C. O'Brien, and G. Faulkner, "Indoor Optical Wireless MIMO Swith an Imaging Receiver," *IEEE photonics technology letters*, vol. 23, no. 2, pp. 97–99, 2011.
[7] R. Y. Mesleh, H. Haas, S. Sinanovic, C. W. Ahn, and S. Yun, "Spatial Modulation," *IEEE Transactions on Vehicular Technology*, vol. 57, no. 4, pp. 2228–2241, 2008.
[8] H. G. Olanrewaju and W. O. Popoola, "Effect of Synchronization Error on Optical Spatial Modulation," *IEEE Transactions on Communications*, vol. 65, no. 12, pp. 5362–5374, Dec 2017.
[9] T. Fath and H. Haas, "Performance Comparison of MIMO Techniques for Optical Wireless Communications in Indoor Environments," *IEEE Transactions on Communications*, vol. 61, no. 2, pp. 733–742, 2013.
[10] T. Fath, M. Di Renzo, and H. Haas, "On the Performance of Space Shift Keying for Optical Wireless Communications," in *2010 IEEE GLOBECOM Workshops (GC Wkshps)*. IEEE, 2010, pp. 990–994.
[11] R. Mesleh, H. Elgala, and H. Haas, "Optical Spatial Modulation," *Journal of Optical Communications and Networking*, vol. 3, no. 3, pp. 234–244, 2011.
[12] W. O. Popoola, E. Poves, and H. Haas, "Spatial Pulse Position Modulation for Optical Communications," *Journal of Lightwave Technology*, vol. 30, no. 18, pp. 2948–2954, 2012.
[13] X. Zhang, S. Dimitrov, S. Sinanovic, and H. Haas, "Optimal Power Allocation in Spatial Modulation OFDM for Visible Light Communications," in *Vehicular Technology Conference (VTC Spring), 2012 IEEE 75th*. IEEE, 2012, pp. 1–5.
[14] M. Di Renzo, H. Haas, A. Ghrayeb, S. Sugiura, and L. Hanzo, "Spatial Modulation for Generalized MIMO: Challenges, Opportunities, and Implementation," *Proceedings of the IEEE*, vol. 102, no. 1, pp. 56–103, 2014.
[15] H. G. Olanrewaju, J. Thompson, and W. O. Popoola, "Generalized Spatial Pulse Position Modulation for Optical Wireless Communications," in *2016 84th IEEE Vehicular Technology Conference (VTC Fall)*. IEEE, 2016.
[16] R. Mesleh, R. Mehmood, H. Elgala, and H. Haas, "Indoor MIMO Optical Wireless Communication using Spatial Modulation," in *2010 IEEE International Conference on Communications (ICC)*. IEEE, 2010, pp. 1–5.
[17] N. A. Tran, D. Luong, T. C. Thang, A. T. Pham *et al.*, "Performance Analysis of Indoor MIMO Visible Light Communication Systems," in *2014 IEEE Fifth International Conference on Communications and Electronics (ICCE)*. IEEE, 2014, pp. 60–64.
[18] W. O. Popoola, E. Poves, and H. Haas, "Error Performance of Generalised Space Shift Keying for Indoor Visible Light Communications," *IEEE Transactions on Communications*, vol. 61, no. 5, pp. 1968–1976, 2013.
[19] S. Rajbhandari, H. Chun, G. Faulkner, K. Cameron, A. V. Jalajakumari, R. Henderson, D. Tsonev, M. Ijaz, Z. Chen, H. Haas *et al.*, "High-Speed Integrated Visible Light Communication System: Device Constraints and Design Considerations," *IEEE Journal on Selected Areas in Communications*, vol. 33, no. 9, pp. 1750–1757, 2015.
[20] D. Tsonev, H. Chun, S. Rajbhandari, J. J. McKendry, S. Videv, E. Gu, M. Haji, S. Watson, A. E. Kelly, G. Faulkner *et al.*, "A 3-Gb/s Single-LED OFDM-based Wireless VLC Link Using a Gallium Nitride μLED," *IEEE Photon. Technol. Lett.*, vol. 26, no. 7, pp. 637–640, 2014.
[21] M. D. Audeh, J. M. Kahn, and J. R. Barry, "Performance of Pulse-position Modulation on Measured Non-Directed Indoor Infrared Channels," *IEEE Transactions on Communications*, vol. 44, no. 6, pp. 654–659, 1996.
[22] J. R. Barry, J. M. Kahn, W. J. Krause, E. A. Lee, and D. G. Messerschmitt, "Simulation of Multipath Impulse Response for Indoor Wireless Optical Channels," *IEEE journal on selected areas in communications*, vol. 11, no. 3, pp. 367–379, 1993.
[23] K. Lee, H. Park, and J. R. Barry, "Indoor Channel Characteristics for Visible Light Communications," *IEEE Communications Letters*, vol. 15, no. 2, pp. 217–219, 2011.
[24] Z. Zhou, C. Chen, and M. Kavehrad, "Impact Analyses of High-Order Light Reflections on Indoor Optical Wireless Channel Model and Calibration," *Journal of Lightwave Technology*, vol. 32, no. 10, pp. 2003–2011, May 2014.
[25] J. M. Kahn and J. R. Barry, "Wireless Infrared Communications," *Proceedings of the IEEE*, vol. 85, no. 2, pp. 265–298, 1997.
[26] J. Proakis and M. Salehi, *Digital Communications*, 5th ed. McGraw-Hill, 2008.
[27] W. O. Popoola and H. Haas, "Demonstration of the Merit and Limitation of Generalised Space Shift Keying for Indoor Visible Light Communications," *Journal of Lightwave Technology*, vol. 32, no. 10, pp. 1960–1965, 2014.

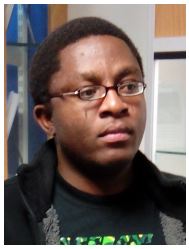

Hammed G. Olanrewaju received his BEng degree with first class (Hons.) in electrical and electronic engineering from the Federal University of Agriculture, Abeokuta, Nigeria, in 2010, and his MSc in Communications and Signal Processing from Imperial College, London, in 2014. He is currently pursuing a Ph.D. degree in the Institute for Digital Communications, School of Engineering at the University of Edinburgh, UK. His research interest includes optical wireless communications, visible light communications, and multiple-input multiple-output (MIMO) systems.

John Thompson is currently a Professor at the School of Engineering in the University of Edinburgh. He specializes in antenna array processing, cooperative communications systems and energy efficient wireless communications. He has published in excess of three hundred papers on these topics, He was coordinator for the recently completed EU Marie Curie Training Network ADVANTAGE, which studies how communications and power engineering can provide future smart grid systems). In 2018, he will be a co-chair of the IEEE Smartgridcomm conference to be held in Aalborg, Denmark. He currently leads two UK research projects which study new concepts for fifth generation wireless communications. In January 2016, he was elevated to Fellow of the IEEE for contributions to antenna arrays and multi-hop communications. In 2015-2017, he has been recognised by Thomson Reuters as a highly cited researcher.

Wasiu O. Popoola holds a first class (Hons.) degree in electronic and electrical engineering from Obafemi Awolowo University, Nigeria, an MSc and a PhD degree, both from Northumbria University in Newcastle upon Tyne, UK. During his PhD, he was awarded the 'Xcel Best Engineering and Technology Student of the year 2009'. He is currently a university lecturer and chancellor's fellow in the Institute for Digital Communications, School of Engineering at the University of Edinburgh, UK. He has published over 80 journal articles/conference papers/patent and over seven of those are invited papers. One of his journal articles ranked No. 2 in terms of the number of full text downloads within IEEE Xplore in 2008, from the hundreds of papers published by IET Optoelectronics since 1980. Another paper he co-authored with one of his PhD students won the best poster award at the 2016 IEEE ICSAE Conference. He also co-authored the book 'Optical Wireless Communications: System and Channel Modelling with MATLAB, published by CRC in 2012, and several other book chapters (one with over 10000 downloads as of Sept. 2014 since its publication in 2010). Popoola is a senior member of the IEEE, an associate editor of the IEEE Access journal and Guest Editor for Elsevier Journal of Optik (special issue on optical wireless communications) in 2017 and Technical Program Committee member for several conferences. He was an invited speaker at various events including the 2016 IEEE Photonics Society Summer Topicals. Popoola has primary research interest in optical communications including visible light communications, free-space optical communication and fibre communication.